CHARACTERISATION OF INFRAGRAVITY WAVES AND THEIR ASSOCIATED HYDRODYNAMICS PROCESSES IN MESO-MACRO TIDAL LAGOON

Paul Bayle, Brgm, Regional Direction Nouvelle-Aquitaine / Ifremer, LITTORAL, F-33120 Arcachon, France p.bayle@brgm.fr
Alexandre Nicolae Lerma, Brgm, Regional Direction Nouvelle-Aquitaine, France, a.nicolaelerma@brgm.fr
Xavier Bertin, UMR 7266 LIENSS, CNRS/Rochelle Université, France, xavier.bertin@univ-lr.fr
Nadia Sénéchal, UMR EPOC/Université de Bordeaux, France, nadia.senechal@u-bordeaux.fr
Florian Ganthy, Ifremer, LITTORAL, F-33120 Arcachon, France florian.ganthy@ifremer.fr

INTRODUCTION

Infragravity (hereafter 'IG') waves are ocean waves related to the presence of groups in incident shortwaves. The importance of IG waves in the nearshore and their role in beach morphodynamics have been widely documented over the last few decades (Bertin *et al.,* 2018) while in contrast, studies on characterisation of IG waves and related impacts in tidal inlets are scarce and have only recently begun to be addressed (Williams and Stacey, 2016). Nonetheless, existing studies tend to show that IG waves in tidal inlets can play an important role in the short and long-term hydro-morphodynamics of coastal lagoons. The current study presents the first large scale field measurements and analysis of IG waves propagation and characteristics in a meso-macro tidal lagoon/inlet.

FIELD MEASUREMENTS

An extensive field campaign was undertaken in the Arcachon lagoon in winter 2021 (Fig 1). Instruments were deployed for six weeks from outside to inside the lagoon, with a particular coverage of the inlet. Over this period, continuous measurements of pressure and currents were performed using Pressure Transducers (blue circles) and Acoustic Doppler Current Profiler (red triangles). For logistics reasons, some points could not be instrumented over the entire period and many were installed in intertidal zones, resulting in a varying spatial and temporal coverage. In this study, the 'ebb tidal data' refer to the shallow sand banks visible seaward point 114 longitude.
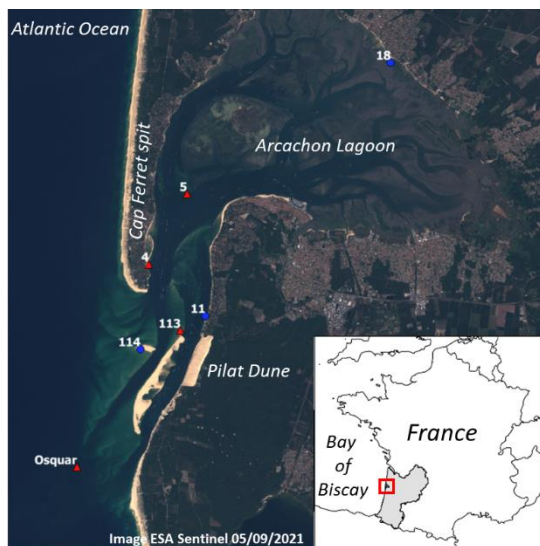

Figure 1 – Location of measurement points. Blue dots mark pressure measurements only and red triangles mark both

current and pressure measurements.

DATA PROCESSING

Surface elevations were obtained from the pressure signal using, based on the type of environment, a linear reconstruction for the points Osquar and 18 and the weakly dispersive method presented by Martins *et al.* (2021) for the others. The high frequency cutoff for the reconstruction was taken at 0.2 Hz for Osquar, and 0.4 Hz for the other points. A high pass filter of 0.0011 Hz (15 minutes) was used to remove free surface oscillations larger than the targeted IG waves. The surface elevation was then segmented into 30-minute burst, and the elevation density spectra were computed using a fast Fourier transform, with 7 Hanning-window, 50 % overlapping segments of 512 seconds. The frequency cutoff (f_c) between IG and gravity waves was time-varying and taken as 0.5 times the discrete peak frequency f_p of a burst (Oh *et al.* 2020). Available current data were extracted across the water column, and used at Osquar to separate the incident and reflected signal, following the method developed by Guza *et al.* (1984).

The 'offshore' environmental conditions are the measurements recorded at Osquar (Fig 2). Note that the grey shaded areas show when short waves are supposed to break (in the form of spilling waves over long distance) at Osquar location. The incident wave angle is nearly normal (280-300°N) relative to the ebb tidal delta and inlet. To study the propagation of IG waves in the lagoon, only the incoming signal - *i.e.*, the part of the signal entering the lagoon - was taken into account. Therefore, only the incident IG signal is used at Osquar (panel 3, Fig 2), while the total IG signal is used at the other points.
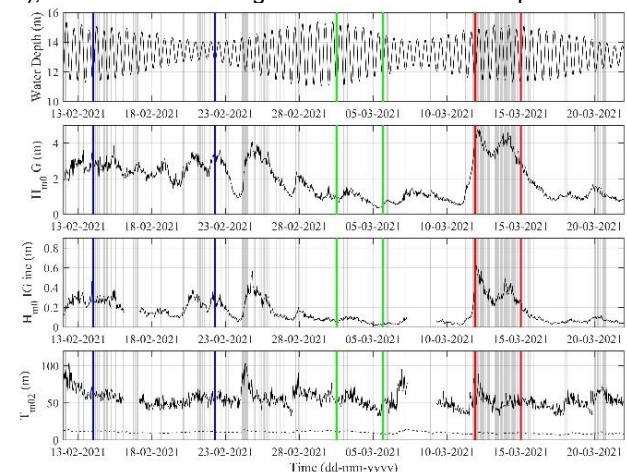

Figure 2 – Measured parameters at Osquar ('offshore'). *From top to bottom*: Water depth; H_{m0} in the gravity band; H_{m0} incident in the infragravity band; and T_{m02} in the gravity

(dashed line) and incident infragravity band (plain line).

HIGH OFFSHORE IG WAVES

Figure 3 focuses on a high IG waves and large tidal range period (red window, Fig 2), and shows the evolution of the IG energy flux, in kw.m^{-1}, given as:

$$P_{IG} = E_{IG} * c_g \qquad (1)$$

with E_{IG} the energy calculated with H_{m0_IG}, and c_g the IG wave group velocity. Note that during this period, the water depth at high tide in the ebb tidal delta is 5 m on average.
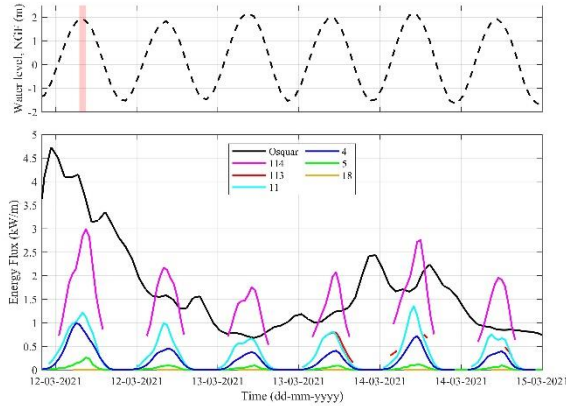

Figure 3 - *Top panel*: Water level at Osquar in France Generalised Elevation (NGF) system, and *Bottom panel*: Energy flux, P_{IG} in the infragravity band, for all the available points during the high IG waves and large tidal range period. The red shaded band marks the high tide one-hour window used in the spectrogram analysis showed in Figure 4.a.

Figure 3 shows that the IG energy flux in the inlet at 114 often exceeds the offshore one at Osquar. The energy flux contained in the IG band increases between offshore and 114, where the depth decreases over the large sand banks forming the ebb tidal delta (Fig 1). Therefore, short waves start breaking earlier and the shoaling zone ends further offshore during energetic conditions than during calm conditions. Therefore, the relative part of the offshore (Osquar)-114 transect comprised in the shoaling zone is more important during moderate-energy wave conditions than high-energy wave conditions. The shoaling zone being where IG waves are expected to receive energy from the short waves through the bound wave mechanism (*e.g.*, Bertin et al., 2020), it is expected to have a significant increase in IG energy during moderate-energy wave conditions (longer shoaling zone) than high energy-wave conditions (shorter shoaling zone). Once short waves group completely break, IG waves stop receiving energy and start dissipating via multiple mechanisms (*e.g.*, dissipation through energy transfer to short waves), that can explain the lower energy at 114 than at Osquar during the first tide in Figure 3.

Furthermore, Figure 3 shows that from 114, the IG energy fluxes then decrease as they propagate in the lagoon. This is further detailed in Figure 4.a which shows the evolution of the energy spectrum over space computed over a one-hour window around the first high tide (Fig 3). It is clear that the total IG energy decreases inward, but yet remains relatively important at the internal part of the inlet (at point 11, 4) and even inside the lagoon (point 5), with H_{m0_IG}

reaching 0.40, 0.37, and 0.15 m respectively. The IG energy fluxes is residual at point 18, with H_{m0_IG} of 3.5 cm. In addition, Figure 4.a shows that IG energy is mainly maintained in low frequencies (from 0.002 to 0.008 Hz) as it propagates. The T_{m02_IG} does not significantly change as IG fluxes propagate, and stay around 80 s. In overall, the energy travelling is mainly contained in the IG band, meaning IG waves dominate the free surface elevation variance in the inlet and lagoon.
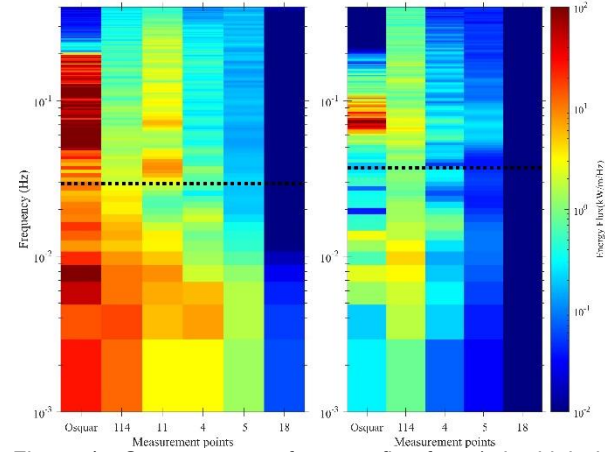

Figure 4 - Spectrograms of energy flux for: a) the high tide one-hour window during the high offshore IG wave period, shown in Fig 3 and b) the high tide one-hour window during the low offshore IG wave period, shown in Fig 5. Note that 11 was not available for the low energy period. The propagation direction on each subplot is from left (outside) to right (inside). The dashed black line shows the adaptive frequency cut-off between infragravity and gravity band.
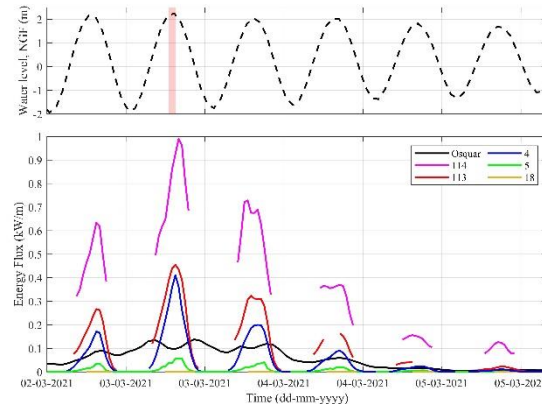
LOW OFFSHORE IG WAVES

Figure 5 - *Top panel*: Water level at Osquar location in NGF referential, and *Bottom panel*: Energy flux, P_{IG} in the infragravity band, for all the available points during the low IG wave and large tidal range period. The red shaded band marks the high tide one-hour window used in the spectrogram analysis showed Figure 4.b.

Figure 5 shows the same parameters as Figure 3, but this time focusing on a low IG waves and large tidal range period (green window, Fig 2). The overall energy flux at 114 is about three times lower than during high offshore IG wave events, however the amplification factor is three

to five times larger. During this low energy-wave conditions (Fig 2), the part of the offshore (Osquar)-114 transect comprised in the shoaling zone is larger than during more energetic conditions as explained in the previous section, and so it is expected to have more energy transfer through the bound wave mechanism. As a result, IG energy fluxes propagating from the inlet to inside the lagoon are larger than the offshore energy fluxes up to somewhere between 4 and 5. The energy fluxes at point 5 are only half of the offshore fluxes while it was more than ten times smaller during high offshore IG waves (Fig 3). In addition, the H_{m0_IG} at point 5 is 7.5 cm so only half of the height measured during the high offshore IG waves period.

Figure 4.b shows the spectrograms for the low IG waves period. It clearly illustrates the energy gain in IG frequencies (mainly around 0.01 Hz and lower) occurring between the offshore and 114. This energy is maintained at point 4 at 0.016 and 0.0056 Hz, but then decreases further inward. The T_{m02_IG} increases gradually by 5-10 s over the basin, varying from 54 to 60 s. In overall, the energy travelling in the lagoon is balanced between infragravity and gravity band, with a sharp decrease in IG energy between point 4 and 5.

During both high (Fig 3) and low (Fig 5) offshore IG period, the IG energy fluxes recorded at low tide submerged points (5 and sometimes 4) where near 0 for all low tides. The residual signal has value of T_{m02_IG} varying from 80 s to 140 s. Note the water depth at low tide in the ebb tidal delta is 1.5 m on average. In consequence, it is hypothesised a combination of IG dissipation through short waves breaking and short IG waves blockage by strong counter-directed ebb currents in very shallow parts of the ebb tidal delta are responsible for the almost total disappearance of IG waves at low tide in the inlet and inside lagoon.
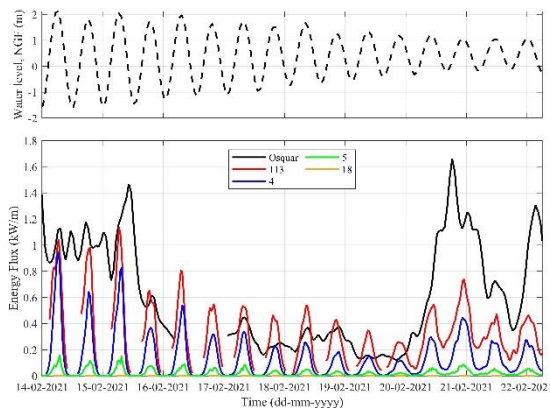
VARYING TIDAL RANGE

Figure 6 - *Top panel*: Water level at Osquar in NGF referential, and *Bottom panel*: Energy flux, P_{IG} in the infragravity band, during the moderate IG waves and varying tidal range period (blue window in Figure 2).

This section focuses on a period where offshore wave conditions are nearly stable but tidal range varies from 3.9 m to 1.3 m. The transition from one to the other is

displayed in Figure 7. It shows that during the large tidal range period, the energy flux variations behave as described in previous sections (Fig 3 and 5), with enhanced energy fluxes propagating at point 113, 4 and 5 during high tide, and almost no IG signal at low tide. However, the pattern is different when the tidal range is smaller. For similar IG energy flux at Osquar (*e.g.* 15/02/21 and 21/02/21), the energy flux at all points at high tide are 1.5 times smaller for the small tidal range than for the large tidal range. Furthermore at low tide, the IG energy flux for the small tidal range is not 0, and even relatively important with H_{m0_IG} reaching 0.22, 0.10, and 0.05 m at point 113, 4 and 5 respectively. The change from one pattern to the other is related to the water depth in the ebb tidal delta, and the control on IG energy flux is progressive and follows the tidal range decrease. For similar offshore conditions, the average energy flux per hour over one day (two complete tidal cycles) is nonetheless near the same for both patterns at 113 (0.75 kW/m/h), 4 (0.40 kW/m/h) and 5 (0.04 kW/m/h), meaning that although the energy do not propagate in the same way, the total energy is the same.

CONCLUSION

This analysis shows that due to energy transfer toward the IG band occurring in the shallow ebb tidal delta, large IG energy fluxes reach the inlet and propagate in the lagoon, with sometimes values in the internal part of the inlet exceeding the offshore ones. It also shows that large IG energy fluxes pass the inlet and dominate the overall inside energy fluxes propagating during energetic offshore IG events. In addition, the analysis revealed that relatively important IG energy fluxes are generated over the ebb delta and propagate inside the lagoon even during low offshore IG wave periods. The combination of water depth in the ebb delta and offshore conditions drive the whole observed IG processes in the inlet and lagoon.

REFERENCES

Bertin, X., Martins, K., de Bakker, A., Chataigner, T., Guérin, T., Coulombier, T., and de Viron, O. (2020). Energy transfers and reflection of infragravity waves at a dissipative beach under storm waves. Journal of Geophysical Research: Oceans, 125.

Bertin, X., de Bakker, A., van Dongeren, A., Coco, G., André, G., Ardhuin, F., Bonneton, P., Bouchette, F., Castelle, B., Crawford, W. C., Davidson, M., Deen, M., Dodet, G., Guérin, T., Inch, K., Leckler, F., McCall, R., Muller, H., Olabarrieta, M., Roelvink, D., Ruessink, G., Sous, D., Stutzmann, É., & Tissier, M. (2018). Infragravity waves: From driving mechanisms to impacts. Earth-Science Reviews, 177, 774-799.

Martins, K., Bonneton, P., Lannes, D. and Michallet, H. (2021). Relation between orbital velocity, pressure, and surface elevation in nonlinear nearshore water waves. Journal of Physical Oceanography, 51, 3539-3556.

Oh, J.E., Jeong, W.M., Chang, S.Y. and Oh, S.H. (2020). On the separation period discriminating gravity and infragravity waves off Gyeongpo beach, Korea. J. of Mar. Sci. and Eng., 8, 167.

Williams, M. E., & Stacey, M. (2016). Tidally discontinuous ocean forcing in bar-built estuaries: The interaction of tides, infragravity motions, and frictional control. Journal of Geophysical Research: Oceans, 121, 571- 585.